Nanoscale

Accepted Manuscript

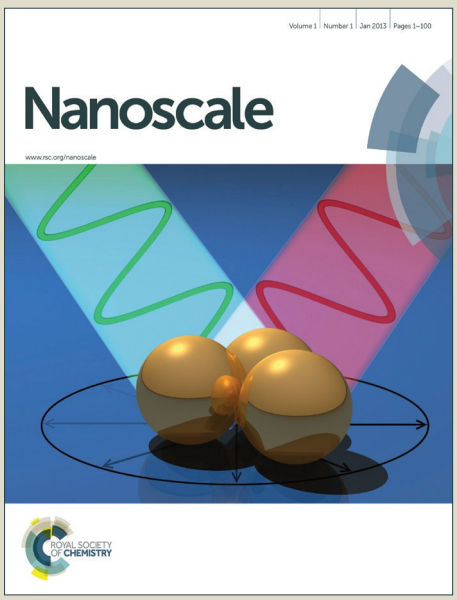

ROYAL SOCIETY OF CHEMISTRY

www.rsc.org/nanoscale

Journal Name

COMMUNICATION

Nanoparticle-mediated photothermal effect enables a new method for quantitative biochemical analysis using a thermometer

Received 00th January 20xx,
Accepted 00th January 20xx

DOI: 10.1039/x0xx00000x

www.rsc.org/

Guanglei Fu,[a] Sharma T. Sanjay,[a] Maowei Dou[a] and XiuJun Li[a,b,c,*]

We have developed a new biomolecular quantitation method, nanoparticle-mediated photothermal bioassay, using a common thermometer as the signal reader. Using immunoassay as a proof of concept, iron oxide nanoparticles (NPs) captured in the sandwich-type assay system are transformed into a near-infrared (NIR) laser-driven photothermal agent, Prussian blue (PB) NPs, which act as a photothermal probe to convert the assay signal into heat through the photothermal effect, thus allowing sensitive biomolecular quantitation using a thermometer. This is the first report of biomolecular quantitation using a thermometer, which also serves as the first attempt to introduce the nanoparticle-mediated photothermal effect for bioassays.

The development of new methods for quantitative detection of biomolecules has been the subject of great research interest especially for disease biomarker detection in clinical diagnosis.[1-3] A number of immunoassays based on different detection principles, such as the traditional enzyme linked immunosorbent assay (ELISA), surface plasmon resonance, surface enhanced Raman scattering, chemiluminescence, electrochemistry and fluorescence methodologies,[4-10] have been widely used in biomolecular detection. Despite of great research progress, these traditional bioassays usually have to be confronted with several limitations especially in resource-limited settings. Typically, one of the most critical bottlenecks is the assay readout method, because most traditional readout methods rely on bulky and expensive analytical equipment.[11] Colorimetric results can be observed by the naked eye for qualitative analysis or semi-quantitative analysis, but the sensitivity of colorimetric detection is low. Further aid of other analytical, imaging and computation equipment is required to achieve quantitative detection. Furthermore, professionally trained personnel for the use of the equipment, software and assay protocols are generally indispensable during these conventional bioassays, further limiting their potential for wide application. Therefore, the development of new cost-effective readout methods for quantitative detection of various biomolecules is in great demand to advance affordable biomolecular quantitation and to address limitations of current methods to improve global health.[12-14]

The study of nanoparticle-mediated photothermal effect has currently emerged as a particularly attractive research topic in various fields because of the unique light-to-heat photo-physical conversion property.[15-17] In particular, near-infrared (NIR) light-driven photothermal effect has shown great promise in biomedical field for non-invasive photothermal therapy of cancers employing heat converted by photothermal agents from NIR light absorption.[18-21] A variety of nanomaterials such as Prussian blue (PB)-, carbon- and gold-based nanomaterials that can convert the NIR light into heat have been developed as photothermal therapeutic agents.[15, 16, 22-26] It is noteworthy that heat generated from the photothermal therapeutic process can be accurately monitored by using a thermometer, one of the most widely-used, portable and inexpensive analytical tools. Hence, introduction of the nanoparticle-mediated photothermal effect in bioassays makes it feasible to develop a novel low-cost approach for biomolecular quantitation using a common thermometer. Although photothermal effect has been extensively studied for photothermal therapy, to the best of our knowledge, the nanoparticle-mediated photothermal effect has never been utilized for quantitative biomolecular detection.

Herein, we have introduced the nanoparticle-mediated photothermal effect to develop a new biomolecular quantitation method, nanoparticle-mediated photothermal bioassay, using a common thermometer as the signal reader for quantitative biomolecular detection. As shown in Figure 1 using a typical sandwich-type immunoassay as the proof of concept, monoclonal antibody was used as the capture antibody pre-immobilized on microcentrifuge tube surface, while iron oxide nanoparticles (Fe_3O_4 NPs)-labelled polyclonal antibody was used as the detection antibody. Different concentrations of cancer biomarkers (antigen)

[a] Department of Chemistry, University of Texas at El Paso, 500 West University Ave, El Paso, Texas, 79968, USA. E-mail: xli4@utep.edu
[b] Biomedical Engineering, University of Texas at El Paso, 500 West University Ave, El Paso, Texas, 79968, USA.
[c] Border Biomedical Research Center, University of Texas at El Paso, 500 West University Ave, El Paso, Texas, 79968, USA.

† Electronic Supplementary Information (ESI) available: Detailed experimental, Figure S1 and Table S1. See DOI: 10.1039/x0xx00000x

were used as the target analyte. After the incubation with antigen and thorough washing, Fe_3O_4 NPs were introduced to form a typical sandwich structure. Because the photothermal effect of Fe_3O_4 NPs was weak, we converted Fe_3O_4 NPs into Prussian blue (PB) NPs for stronger photothermal effect. Fe_3O_4 NPs captured in the sandwich-type immunoassay system were then dissolved in an acidic condition to release ferric ions, followed by reactions with potassium ferrocyanide to produce PB NPs, a NIR laser-driven photothermal agent. The as-obtained PB NPs act as a highly sensitive photothermal probe to convert the immunoassay signal into heat through their NIR laser-driven photothermal effect, thus allowing sensitive and quantitative readout of the immunoassay by using a common thermometer. Using Prostate-specific antigen (PSA) as the analyte, the photothermal effect, specificity and reliability of the developed photothermal immunoassay were studied systematically. To the best of our knowledge, this is the first attempt to introduce the nanoparticle-mediated photothermal effect for biomolecular quantitation. Most importantly, the innovative application of the nanoparticle-mediated photothermal effect has enabled a new biomolecular quantitation strategy using a common thermometer, thus providing new opportunities toward advances in the development of affordable bioassays, particularly in low-resource settings.

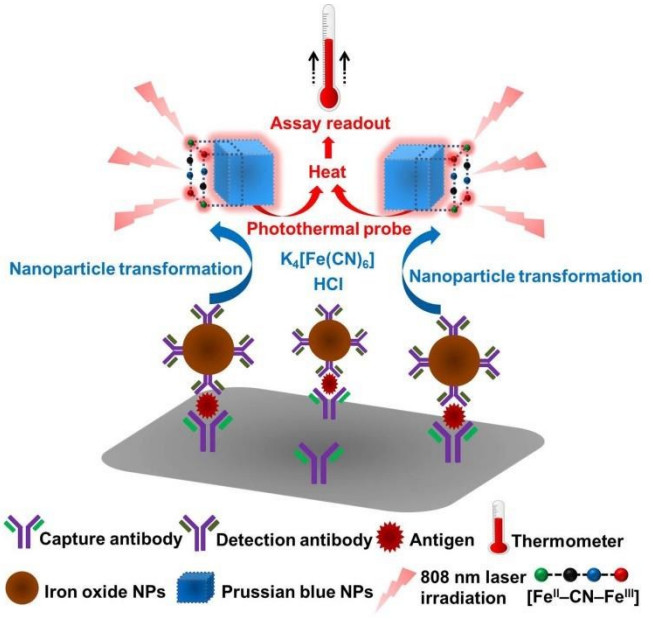

Fig. 1 Schematic illustration of the nanoparticle-mediated photothermal immunoassay using a common thermometer as the quantitative signal reader.

PB as an ancient dye is a prototype of mixed-valence transition metal hexacyanoferrates.[27] Owing to their strong optical absorption in the NIR region and high photothermal efficiency, recently, PB NPs have been explored as a new generation of NIR laser-driven photothermal agent.[15, 28]

To confirm the production of PB NPs in the immunoassay solution after the nanoparticle transformation process, UV-Vis spectroscopic characterization was carried out before and after the reaction with potassium ferrocyanide. As expected, clear color change of the immunoassay solution to blue was observed at a PSA concentration of 32.0 ng·mL^{-1} after the nanoparticle transformation process (Figure 2A), corresponding to the typical blue color of PB. Meanwhile, a broad absorption peak at 748 nm in the UV-Vis spectra of the immunoassay solution (32.0 ng·mL^{-1} PSA) was observed after the transformation process (Figure 2B), while no absorption peak was exhibited before the process. The absorption peak corresponded well with that of PB NPs due to the charge transfer transition between Fe (II) and Fe (III) in PB,[15, 16] indicating the generation of PB in the immunoassay solution after the nanoparticle transformation process. The slight redshift of the absorption peak of PB in the immunoassay solution might be attributed to the different matrix effect from the immunoassay solution. In addition, no apparent absorption peak (Figure 2B) and color change (Figure 2A) were observed even after the nanoparticle transformation process in the absence of target PSA, because no Fe_3O_4 NPs were captured in the sandwich-type immunoassay system in the absence of target PSA, and thus no PB would be generated in the control solutions. These results confirmed the production of PB in the immunoassay solution.

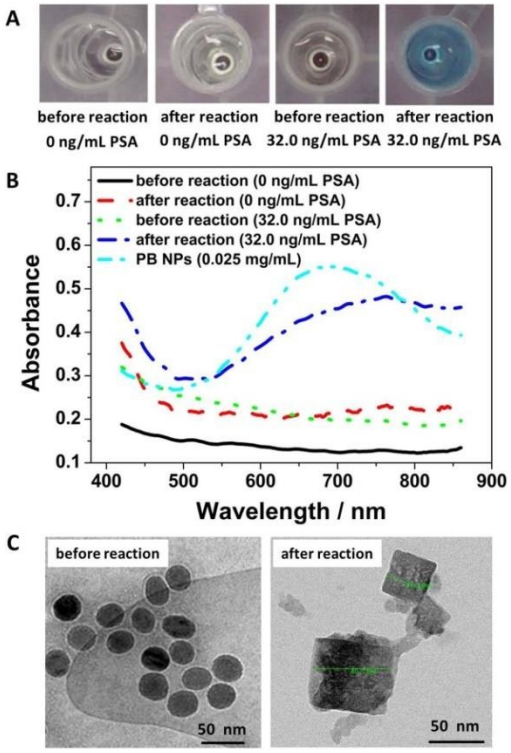

Fig. 2 Photographs (A) and UV-Vis spectra (B) of the immunoassay solutions at different PSA concentrations before and after the reaction with potassium ferrocyanide. (C) TEM images of nanoparticles in the immunoassay solutions at a PSA concentration of 32.0 ng·mL^{-1} before and after the nanoparticle transformation process.

To further confirm the production of PB NPs in the immunoassay solution, Transmission electron microscopy (TEM) and Fourier transform infrared spectroscopy (FTIR, see Figure S1 in the Supporting Information) were performed to characterize the change of nanoparticles in the immunoassay solution at a PSA concentration of 32.0 ng·mL^{-1} before and after the nanoparticle transformation process. Fe_3O_4 NPs captured in the sandwich-type immunoassay system were collected for TEM observation prior to the dissolution procedure in the acidic condition. Nanoparticles with uniformly spherical morphology at an average diameter of 40

nm were observed in the TEM image (Figure 2C), which corresponded well with the product information from the manufacture (Ocean NanoTech LLC, USA). However, an obvious change in morphology was observed after the nanoparticle transformation process (Figure 2C). With the disappearance of the spherical iron oxide NPs, nanoparticles with clear cubic morphology in the size range from 20 to 100 nm were observed in the TEM image, which was in good agreement with the well-known cubic morphology of PB NPs.[15, 29, 30] The result further confirmed the successful Fe_3O_4-to-PB NPs transformation in the immunoassay solution.

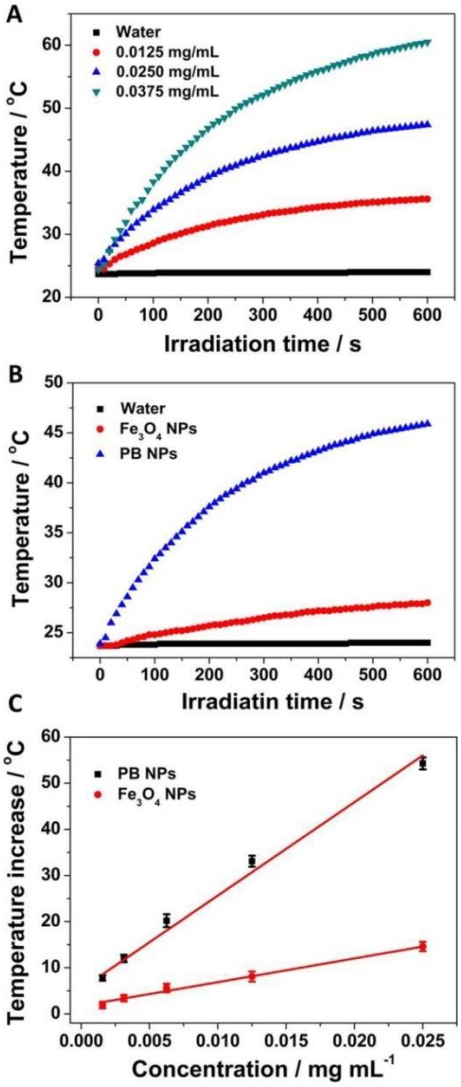

Fig. 3 (A) Temperature comparison among water and different concentrations of PB NPs using a common thermometer during the irradiation of a 808 nm laser at a power density of 3.12 W·cm^{-2} for 10 min. (B) Temperature comparison among water, Fe_3O_4 NPs (0.025 mg·mL^{-1}) and PB NPs (0.025 mg·mL^{-1}) during the irradiation for 10 min. (C) Temperature increase (ΔT) measured by a thermometer vs. concentrations of Fe_3O_4 NPs and PB NPs after the irradiation of a 808 nm laser at a power density of 5.26 W·cm^{-2} for 1.5 min.

To investigate the feasibility of PB NPs for photothermal immunoassay, NIR laser-driven photothermal effect of PB NPs was first studied. Using water as the control, aqueous dispersions (1.0 mL) of different concentrations of PB NPs were irradiated by a 808 nm laser for 10 min at a power density of 3.12 W·cm^{-2}. A pen-style digital thermometer was used to monitor the temperature of the dispersions during the irradiation process. Figure 3A shows the temperature change of the dispersions during the process. The PB NPs dispersions showed a dramatic temperature increase during the irradiation process, while no significant temperature change was observed for water. It can be found that the higher concentrations of PB NPs ranging from 0.0125 to 0.0375 mg·mL^{-1}, the higher temperature was recorded. PB NPs at a low concentration of 0.0125 mg·mL^{-1} can lead to a temperature elevation of 11.3 °C. Surprisingly, 0.0375 mg·mL^{-1} PB NPs dispersion reached a high temperature increase up to 36.3 °C after the irradiation process! Moreover, irradiation for only 1.0 min can result in a rapid temperature elevation of 10.0 °C at 0.0375 mg·mL^{-1}. The result demonstrated considerable photothermal effect of PB NPs upon the irradiation of NIR laser, which is attributed to their strong optical absorption in the NIR region due to the charge transfer transition between Fe (II) and Fe (III) in PB NPs.[31]

To evaluate the photothermal effect before and after the Fe_3O_4-to-PB NPs transformation process, photothermal effect of Fe_3O_4 NPs was studied in comparison with that of PB NPs. Figure 3B shows the temperature change of the same concentration (0.025 mg·mL^{-1}) of Fe_3O_4 NPs and PB NPs during the irradiation process (808 nm, 3.12 W·cm^{-2}) for 10 min. As can been seen, Fe_3O_4 NPs showed a minor temperature elevation of 4.3 °C after the irradiation, indicating weak photothermal effect of Fe_3O_4 NPs upon NIR laser irradiation. However, PB NPs showed a 5.2-fold higher temperature increase (22.5 °C) than Fe_3O_4 NPs, which indicated much stronger photothermal effect of PB NPs than Fe_3O_4 NPs. Therefore, the stronger photothermal effect obtained from the Fe_3O_4-to-PB NPs transformation process makes it feasible to use a common thermometer for high-sensitivity photothermal detection. This is the main reason that we transformed Fe_3O_4 NPs to PB NPs in the immunoassay.

To demonstrate the feasibility of the photothermal strategy for quantitative analysis, the relationship between the photothermal effect-induced temperature increase and the concentration of PB NPs was studied. Aqueous dispersions (0.15 mL) of different concentrations of PB NPs were exposed to the laser (5.26 W·cm^{-2}) for 1.5 min. Figure 3C shows different temperature increases (ΔT) versus different concentrations of PB NPs and Fe_3O_4 NPs. As PB NPs concentration increased, the temperature increased dramatically after the irradiation. Significantly, the temperature increase exhibited a linear relationship with the concentration in the range from 0.00156 to 0.0250 mg·mL^{-1} with the square of correlation coefficient of 0.99. Furthermore, temperature measurement of eight 0.0125 mg·mL^{-1}PB NPs dispersions showed a low relative standard deviation (RSD) of 2.16%, implying good reproducibility of the thermometer for readout of the photothermal effect. For comparison, the same concentrations of Fe_3O_4 NPs were also irradiated to study the temperature elevation. Although Fe_3O_4 NPs showed a linear relationship between the temperature increase and its concentration, only a 4.0-fold lower sensitivity than that of PB NPs was achieved due to the weak photothermal effect of Fe_3O_4 NPs. Overall, these series of systematic study indicated the great potential of the photothermal strategy for quantitative detection of PSA and other bioassays using a common thermometer as the assay signal reader.

On such a basis, complete photothermal immunoassay was performed with a common thermometer as the signal reader as illustrated in Figure 1. After the Fe_3O_4-to-PB NPs transformation procedure, different immunoassay solutions obtained from different concentrations of PSA in the range from 1.0 to 64.0 ng·mL^{-1} were irradiated (5.26 W·cm^{-2}) for 1.5 min, and the photothermal effect-induced temperature increase was measured using the pen-style digital thermometer. Figure 4A shows the temperature increase of the immunoassay solutions before and after the Fe_3O_4-to-PB NPs transformation as a function of PSA concentrations. As the PSA concentration increased, a dramatic increase in temperature was observed after the irradiation. An extraordinarily high temperature increase of 38.3 °C from 64.0 ng·mL^{-1} PSA was measured, while an obvious temperature increase of 1.8 °C was observed even at 1.0 ng·mL^{-1} PSA, revealing high sensitivity of the PB NPs-based photothermal immunoassay (after nanoparticle transformation). However, similar to Figure 3C, only minor temperature increases were recorded from the Fe_3O_4 NPs-based photothermal immunoassay (before nanoparticle transformation) even at the high concentration of 64.0 ng·mL^{-1} PSA (6.0 °C).

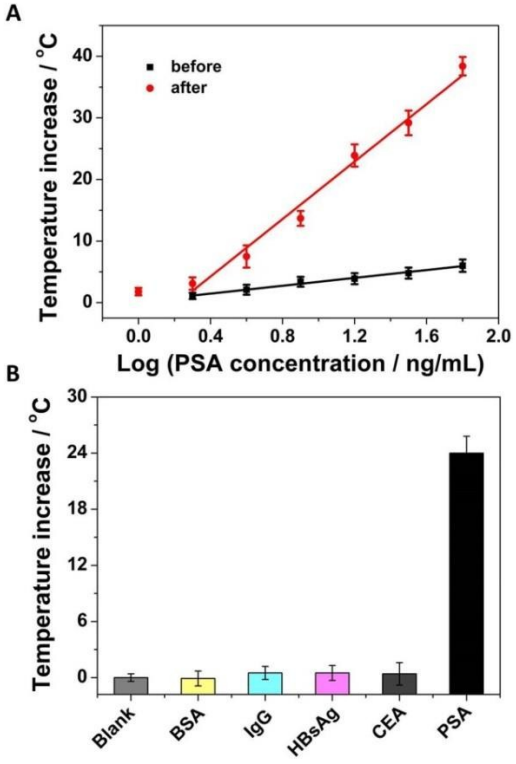

Fig. 4 (A) Calibration plot of temperature increase (ΔT) vs. logarithm of PSA concentration from immunoassay solutions before and after the Fe_3O_4-to-PB NPs transformation process. (B) Specificity test of the photothermal immunoassay method with a thermometer as the signal reader. The concentrations of BSA, CEA, IgG, HBsAg and PSA are 16 μg·mL^{-1}, 160 ng·mL^{-1}, 160 ng·mL^{-1}, 160 ng·mL^{-1} and 16.0 ng·mL^{-1}, respectively.

It was also found from Figure 4A that the temperature increases from both Fe_3O_4 and PB NPs-based photothermal immunoassays were proportional to the logarithm of PSA concentrations in the range from 2.0 to 64.0 ng·mL^{-1} with the squares of correlation coefficients of 0.99 ($Y(^{o}C)=3.15\cdot LogC_{PSA}(ng\cdot mL^{-1})+0.245$) and 0.98 ($Y(^{o}C)=23.3\cdot LogC_{PSA}$ (ng·mL^{-1})-5.08), respectively. Therefore, a 7.4-fold higher slope was obtained as a result of the Fe_3O_4-to-PB NPs transformation. With only a common thermometer for quantitative readout in the photothermal immunoassay, PSA can be determined at the limit of detection (LOD) of 1.0 ng·mL^{-1} without the aid of any advanced analytical equipment. Although this concentration is relatively higher than that of some traditional methods such as electrochemical and fluorescent methods,[32-34] it is comparable to the conventional ELISA method (LOD: 1.0 ng·mL^{-1}) and commercial PSA ELISA kits (LOD: 1.0 ng·mL^{-1}, Biocell Biotechnol. Co., Ltd., Zhengzhou, China) using UV-Vis spectrometers, as reported previously in the literature.[35] In addition, it is noteworthy that the developed photothermal immunoassay can completely meet the requirement of clinical prostate cancer diagnostics, because the threshold concentration of the total PSA in human serum in prostate cancer diagnostics is 4.0 ng·mL^{-1}.[35, 36]

To evaluate the specificity of the developed photothermal immunoassay, some common interfering substances including carcinoembryonic antigen (CEA), immunoglobulin G (IgG), hepatitis B surface antigen (HBsAg) and bovine serum albumin (BSA) were tested. As shown in Figure 4B, a high temperature elevation of 23.9 °C was observed from target PSA (16.0 ng·mL^{-1}), while no significant temperature increase was observed from other interfering substances even with 10-fold higher concentrations, indicating high specificity of our photothermal immunoassay. Along with the specificity, the reproducibility of the photothermal immunoassay was studied by measuring the temperature elevation of six immunoassay solutions obtained from the same PSA concentration (64.0 ng·mL^{-1}). The RSD was 5.19%, indicating acceptable reproducibility of the developed photothermal immunoassay.

To validate the analytical reliability of the developed photothermal immunoassay in the detection of real human samples, normal human serum samples were spiked with different concentrations of PSA for photothermal determination. The recoveries of target PSA spiked in three serum samples were estimated using the thermometer-based readout method. Table S1 shows that all the percent recoveries fall in the range of 91.7-95.8%. These recoveries are comparable to those of some standard commercial PSA ELISA kits (e.g. 94-112% from Abcam, USA and 95-100% from USBio, USA) according to their product information. These results demonstrated acceptable analytical reliability of the developed photothermal immunoassay for detection of real human serum samples.[37]

Conclusions

In summary, based on the nanoparticle-mediated photothermal effect, we have developed a new photothermal biomolecular quantitation method using a common thermometer as the quantitative signal reader. Although the nanoparticle-mediated photothermal effect has been extensively studied in disease therapy, this work serves as the first attempt to introduce it in bioassays for quantitation of various disease biomarkers and proteins. The thermometer-based readout method is not only low-cost, portable and widely-available, but also requires minimal professional training in the use of a thermometer and in data readout, without the need of any specialized software for equipment control and data processing. Furthermore, given many

small, lightweight, powerful and portable NIR laser systems become commercially available, some handheld laser pointers could be used as the light source in our photothermal detection method for point of care application. Most importantly, the innovative application of the nanoparticle-mediated photothermal effect will provide new opportunities toward advances in affordable biomolecular detection possibly even by non-professional people in various public venues, especially in low-resource settings such as developing nations. We envision that the photothermal biomolecular detection strategy will have broad applications ranging from clinical disease diagnosis to various biochemical analysis.

Supporting Information

Additional information on FTIR characterization (Figure S1), photothermal immunoassay of PSA in human serum samples (Table S1), and the experimental section including preparation of antibody-conjugated iron oxide NPs, sandwich-type immunoassay, characterization, and photothermal detection protocol.

Acknowledgements

We would like to acknowledge the financial support from the National Institute of General Medical Sciences of the NIH (SC2GM105584) and the National Institute of Allergy and Infectious Disease of the NIH (R21AI107415). Financial support from NIH RCMI for the BBRC Pilot grant, the University of Texas at El Paso (UTEP) for the IDR Program, Multidisciplinary Research Award Program (MRAP) and URI Program, University of Texas (UT) System for the STARS award, is also greatly acknowledged. We are also grateful to the support from Dr. Chuan Xiao's Group at UTEP for the UV-Vis spectroscopic measurement and Dr. Bernal's group at UTEP for TEM images.

Notes and references

1 L. Gervais, N. de Rooij and E. Delamarche, *Adv. Mater.*, 2011, **23**, H151-H176.
2 S. T. Sanjay, G. L. Fu, M. W. Dou, F. Xu, R. T. Liu, H. Qi and X. J. Li, *Analyst*, 2015, **140**, 7062-7081.
3 P. Zuo, X. J. Li, D. C. Dominguez and B. C. Ye, *Lab Chip*, 2013, **13**, 3921-3928.
4 H. Akhavan-Tafti, D. G. Binger, J. J. Blackwood, Y. Chen, R. S. Creager, R. de Silva, R. A. Eickholt, J. E. Gaibor, R. S. Handley, K. P. Kapsner, S. K. Lopac, M. E. Mazelis, T. L. McLernon, J. D. Mendoza, B. H. Odegaard, S. G. Reddy, M. Salvati, B. A. Schoenfelner, N. Shapir, K. R. Shelly, J. C. Todtleben, G. P. Wang and W. H. Xie, *J. Am. Chem. Soc.*, 2013, **135**, 4191-4194.
5 H. Y. Liu, R. Malhotra, M. W. Peczuh and J. F. Rusling, *Anal. Chem.*, 2010, **82**, 5865-5871.
6 J. R. Prensner, M. A. Rubin, J. T. Wei and A. M. Chinnaiyan, *Sci. Transl. Med.*, 2012, **4**, 127rv123-127rv123.
7 W. Li, M. Li, S. Ge, M. Yan, J. Huang and J. Yu, *Anal. Chem. Acta*, 2013, **767**, 66-74.
8 T. Vo-Dinh, A. M. Fales, G. D. Griffin, C. G. Khoury, Y. Liu, H. Ngo, S. J. Norton, J. K. Register, H. N. Wang and H. Yuan, *Nanoscale*, 2013, **5**, 10127-10140.
9 J. S. Wang and X. G. Qu, *Nanoscale*, 2013, **5**, 3589-3600.
10 X. Li, Z. Nie, C. Cheng, A. Goodale and G. Whitesides, *Proc. Micro Total Analysis Systems*, 2010, **14**, 1487-1489.
11 W. S. Qu, Y. Y. Liu, D. B. Liu, Z. Wang and X. Y. Jiang, *Angew. Chem. Int. Edit.*, 2011, **50**, 3442-3445.
12 A. D. Warren, G. A. Kwong, D. K. Wood, K. Y. Lin and S. N. Bhatia, *Proc. Natl. Acad. Sci. U.S.A.*, 2014, **111**, 3671-3676.
13 M. W. Dou, D. C. Dominguez, X. J. Li, J. Sanchez and G. Scott, *Anal. Chem.*, 2014, **86**, 7978-7986.
14 M. W. Dou, S. T. Sanjay, M. Benhabib, F. Xu and X. J. Li, *Talanta*, 2015, **145**, 43-54.
15 G. L. Fu, W. Liu, S. S. Feng and X. L. Yue, *Chem. Commun.*, 2012, **48**, 11567-11569.
16 G. L. Fu, W. Liu, Y. Y. Li, Y. S. Jin, L. D. Jiang, X. L. Liang, S. S. Feng and Z. F. Dai, *Bioconjugate Chem.*, 2014, **25**, 1655-1663.
17 K. Dong, Z. Liu, Z. H. Li, J. S. Ren and X. G. Qu, *Adv. Mater.*, 2013, **25**, 4452-4458.
18 K. Yang, H. Xu, L. Cheng, C. Y. Sun, J. Wang and Z. Liu, *Adv. Mater.*, 2012, **24**, 5586-5592.
19 X. J. Wu, M. Z. Yu, B. J. Lin, H. J. Xing, J. H. Han and S. F. Han, *Chem. Sci.*, 2015, **6**, 798-803.
20 H. Deng, F. Y. Dai, G. H. Ma and X. Zhang, *Adv. Mater.*, 2015, **27**, 3645-3653.
21 D. Jaque, L. M. Maestro, B. del Rosal, P. Haro-Gonzalez, A. Benayas, J. L. Plaza, E. M. Rodriguez and J. G. Sole, *Nanoscale*, 2014, **6**, 9494-9530.
22 H. K. Moon, S. H. Lee and H. C. Choi, *ACS Nano*, 2009, **3**, 3707-3713.
23 C. Ungureanu, R. Kroes, W. Petersen, T. A. M. Groothuis, F. Ungureanu, H. Janssen, F. W. B. van Leeuwen, R. P. H. Kooyman, S. Manohar and T. G. van Leeuwen, *Nano Lett.*, 2011, **11**, 1887-1894.
24 H. Li, L. L. Tan, P. Jia, Q. L. Li, Y. L. Sun, J. Zhang, Y. Q. Ning, J. H. Yu and Y. W. Yang, *Chem. Sci.*, 2014, **5**, 2804-2808.
25 L. Y. Feng, L. Wu and X. G. Qu, *Adv Mater*, 2013, **25**, 168-186.
26B. Li, Q. Wang, R. J. Zou, X. J. Liu, K. B. Xu, W. Y. Li and J. Q. Hu, *Nanoscale*, 2014, **6**, 3274-3282.
27 G. Zhao, J. J. Feng, Q. L. Zhang, S. P. Li and H. Y. Chen, *Chem. Mater.*, 2005, **17**, 3154-3159.
28X. D. Li, X. L. Liang, F. Ma, L. J. Jing, L. Lin, Y. B. Yang, S. S. Feng, G. L. Fu, X. L. Yue and Z. F. Dai, *Colloids Surf. B Biointerfaces*, 2014, **123**, 629-638.
29 M. Shokouhimehr, E. S. Soehnlen, J. H. Hao, M. Griswold, C. Flask, X. D. Fan, J. P. Basilion, S. Basu and S. P. D. Huang, *J. Mater. Chem.*, 2010, **20**, 5251-5259.
30 M. Hu, S. Furukawa, R. Ohtani, H. Sukegawa, Y. Nemoto, J. Reboul, S. Kitagawa and Y. Yamauchi, *Angew. Chem. Int. Edit.*, 2012, **51**, 984-988.
31 L. Cheng, H. Gong, W. W. Zhu, J. J. Liu, X. Y. Wang, G. Liu and Z. Liu, *Biomaterials*, 2014, **35**, 9844-9852.
32 X. Q. Chen, G. B. Zhou, P. Song, J. J. Wang, J. M. Gao, J. X. Lu, C. H. Fan and X. L. Zuo, *Anal. Chem.*, 2014, **86**, 7337-7342.
33 J. H. Choi, H. S. Kim, J. W. Choi, J. W. Hong, Y. K. Kim and B. K. Oh, *Biosens. Bioelectron.*, 2013, **49**, 415-419.
34 J. Liu, C. Y. Lu, H. Zhou, J. J. Xu, Z. H. Wang and H. Y. Chen, *Chem. Commun.*, 2013, **49**, 6602-6604.
35 Z. Q. Gao, L. Hou, M. D. Xu and D. P. Tang, *Sci. Rep.*, 2014, **4**, 3966.
36 J. Lee, P. Dak, Y. Lee, H. Park, W. Choi, M. A. Alam and S. Kim, *Sci. Rep.*, 2014, **4**, 7352.
37 S. Y. Zhou, W. Zheng, Z. Chen, D. T. Tu, Y. S. Liu, E. Ma, R. F. Li, H. M. Zhu, M. D. Huang and X. Y. Chen, *Angew. Chem. Int. Edit.*, 2014, **53**, 12498-12502.